Human Molecular Genetics, 2017, Vol. 26, No. 12 2277–2289

doi: 10.1093/hmg/ddx118
Advance Access Publication Date: 3 April 2017
Original Article

ORIGINAL ARTICLE

Shortened primary cilium length and dysregulated Sonic hedgehog signaling in Niemann-Pick C1 disease

Sonia Canterini[1], Jessica Dragotto[1], Andrea Dardis[2], Stefania Zampieri[2], Maria Egle De Stefano[3], Franco Mangia[1], Robert P. Erickson[4] and Maria Teresa Fiorenza[1,5,*]

[1]Department of Psychology, Section of Neuroscience and Center for Research in Neurobiology 'Daniel Bovet', Sapienza University of Rome, 00185 Rome, Italy, [2]Regional Coordinator Centre for Rare Diseases, University Hospital Santa Maria della Misericordia, Udine, Italy, [3]Istituto Pasteur Italia-Fondazione Cenci Bolognetti, Department of Biology and Biotechnology 'Charles Darwin' and Center for Research in Neurobiology 'Daniel Bovet', Sapienza University of Rome, Italy, [4]Department of Pediatrics, University of Arizona, Tucson, AZ 85724-5073, USA and [5]IRCCS Fondazione Santa Lucia, 00179 Rome, Italy

*To whom correspondence should be addressed. Tel: +39 06 49917869; Fax: +39 06 49917871; Email: mariateresa.fiorenza@uniroma1.it

Abstract

The Niemann-Pick type C1 (NPC1) disease is a neurodegenerative lysosomal storage disorder due to mutations in the *NPC1* gene, encoding a transmembrane protein related to the Sonic hedgehog (Shh) receptor, Patched, and involved in intracellular trafficking of cholesterol. We have recently found that the proliferation of cerebellar granule neuron precursors is significantly reduced in *Npc1*$^{-/-}$ mice due to the downregulation of Shh expression. This finding prompted us to analyze the formation of the primary cilium, a non-motile organelle that is specialized for Shh signal transduction and responsible, when defective, for several human genetic disorders. In this study, we show that the expression and subcellular localization of Shh effectors and ciliary proteins are severely disturbed in Npc1-deficient mice. The dysregulation of Shh signaling is associated with a shortening of the primary cilium length and with a reduction of the fraction of ciliated cells in Npc1-deficient mouse brains and the human fibroblasts of NPC1 patients. These defects are prevented by treatment with 2-hydroxypropyl-β-cyclodextrin, a promising therapy currently under clinical investigation. Our findings indicate that defective Shh signaling is responsible for abnormal morphogenesis of the cerebellum of Npc1-deficient mice and show, for the first time, that the formation of the primary cilium is altered in NPC1 disease.

Introduction

The Niemann-Pick type C1 (NPC1) disease is an autosomal recessive disorder of cholesterol storage caused by the mutation of either the *NPC1* or *NPC2* genes, encoding for proteins that cooperatively mediate the egress of cholesterol from endosomes/lysosomes (1–4). The deficiency of either protein leads to the accumulation of endocytosed, unesterified cholesterol and of several sphingolipids within the late endosomal/lysosomal (LE/Ly) compartment (2,3), decreasing the metabolic active pool of unesterified cholesterol in the cytosol. The disease is considered a disease of neurodegeneration (5,6). In fact it has been called 'juvenile Alzheimer's' (7) because of its shared characteristics, including abnormal cholesterol metabolism, neurofibrillary tangles, increased levels of amyloid beta (8) and TDP-43 proteinopathy (9).

Most of NPC1 defects are prevented by early treatment with 2-hydroxypropyl-β-cyclodextrin (CD). It was clear from the first

Received: January 13, 2017. **Revised:** March 23, 2017. **Accepted:** March 25, 2017

© The Author 2017. Published by Oxford University Press. All rights reserved. For Permissions, please email: journals.permissions@oup.com

Downloaded from https://academic.oup.com/hmg/article/26/12/2277/3098490 by U.S. Department of Justice user on 17 August 2022

report, using somatic delivery of cyclodextrins in a mouse model of NPC1 that highly significant delays in the onset of symptoms occurred, even though the blood brain barrier (BBB) was found to block the drug (10). When somatic treatment was initiated at postnatal day 7, when the BBB is not fully formed in the mouse, and higher doses were used, the results were more dramatic (11). The effects are well seen in the developing cerebellum where nearly complete correction of the developmental defects occurs (12,13).

The disease is also a disorder of development with altered morphogenesis. This is particularly true of the cerebellum, in which several anomalies of glial cell differentiation and derangement of synaptic input to Purkinje cells (PCs) are responsible for a delay in the acquisition of complex motor skills in pre-puberal Npc1-deficient mice, and may contribute to the later PC degeneration (13). Moreover, significantly reduced *Sonic hedgehog (Shh)* mRNA levels at the time of terminal granule cell precursor divisions cause a reduction in cerebellar lobule size at the end of cerebellar development (12).

There is abundant evidence for the role that Shh signaling plays in cerebellum development (14–16). In vertebrates, Shh mostly acts at the level of primary cilium, a microtubule-based plasma membrane protrusion. Defects in the formation and structure of primary cilium are associated with syndromes with altered cerebellar morphogenesis (17). Patched (Ptch), the Shh receptor, localizes on the plasma membrane of the cilium base and axoneme and prevents the activation of Smoothened (Smo), retaining it within intracellular vesicles. Once bound to Shh, Ptch is removed from the cilia membrane and the inhibition of Smo is relieved, allowing Smo to localize at the cilium membrane, while the Shh-Ptch complex is internalized and degraded by lysosomes (reviewed in Ref. 18). The mechanism responsible for the relief of Smo inhibition in consequence of Shh binding to Ptch still needs clarification, although evidence indicates that it depends on the activity of small molecules of lipid origin, the availability of which is controlled by Ptch (19,20). A key role in the control of Shh signaling is played by the kinesin Kif7, an anterograde motor protein that was recently shown to localize at the cilium tip, where it controls cilium length and structure (21). Kif7 mediates the activation and translocation of Gli (glioma-associated) proteins to the tip of the cilium by physically interacting with Gli transcription factors and influencing their processing (22). In vertebrates, the zinc-finger transcription factors Gli1, Gli2 and Gli3 are the effectors of Shh signaling (23), controlling the expression of genes involved in cell proliferation and cell cycle progression (24). Gli1 and Gli2 usually act as transcriptional activators and full-length or a truncated form of Gli3, as transcriptional activator or repressor, respectively (25–27).

A possible effect of NPC1 deficiency on Shh signaling was previously hypothesized in light of the covalent attachment of a cholesterol moiety to the C-terminus of the proteolytically generated active Shh fragment (28). The presence in the NPC1 protein of a sterol-sensing domain with homology to Ptch (29) also heightened interest in a possible role of Shh signaling in the disease. Furthermore, it was shown that NPC1 trafficking antagonists are weak Shh inhibitors (30). However, the fact that NPC1 patients and mice do not display severe birth defects, e.g. holoprosencephaly, cyclopia and limb deficiencies, typically observed in *Shh* knockout mice (31,32) and patients carrying mutations in the *SHH* gene (33), suggests that SHH signaling is not completely deficient in NPC1 disease. Recently, a mouse model carrying a mutation in the NAD(P) dependent steroid dehydrogenase-like (*Nsdhl*) gene, therefore affecting the cholesterol synthesis pathway, has been exploited to show that cholesterol has an essential role in Shh signaling also in cerebellar granule cell precursors (34). Without cholesterol, there was a significant decrease in granule cell proliferation, as we observed in the *Npc1*$^{-/-}$ mice (12), and as might be expected in NPC1 deficiency where intracellular cholesterol transport is altered, potentially decreasing cholesterol availability for regulatory mechanisms. Among these, the regulation of cell cycle progression (35) and the Shh signal transduction *per se* (36) are likely candidates. In fact, the activity of the two main effectors of Shh pathway, Ptch and Smo is tightly linked to cholesterol metabolism. Ptch inhibits the enrichment of Smo at the plasma membrane by modulating the intracellular concentration of cholesterol (37). Oxysterols, cholesterol derivatives, promote the translocation of Smo to the primary cilium (38) and are emerging as crucial modulators of Smo activity (39,40).

We now present evidence that the expression and subcellular localization of Shh effectors and ciliary proteins are severely disturbed in Npc1-deficient mice. We also present evidence of shortened primary cilia in NPC1 mouse model brains and fibroblasts from NPC1 patients, providing further support to the idea of Shh signaling deficiency in the developing cerebellum of NPC1 model mice.

Results

Altered expression of Shh downstream effectors

Previous data obtained in our laboratory showed that a significant reduction of *Shh* transcripts correlates with the defective proliferation of granule neuron precursors in the cerebella of 2-week-old Npc1-deficient mice, allowing us to trace the onset of this defect between PN12 and PN14 (12). To better characterize the likely contribution of anomalous Shh signaling to this defect, we have now determined whether the Npc1-deficiency affects the expression of Shh effectors, including Ptch, Smo, Kif7 and Gli1, Gli2 and Gli3. We analyzed the level of transcripts mentioned above on PN12 mouse cerebella by real time reverse transcriptase polymerase chain reaction (RT-PCR), observing that the deficiency of Npc1 was associated with a severe dysregulation of the expression of all components analyzed. In particular, the expression levels of Ptch, Smo and Gli3 were significantly reduced, whereas those of Gli1, Gli2 and Kif7 were significantly increased (Fig. 1). The administration of CD to Npc1-deficient mice re-established the expression of all factors to levels similar to those of *wt* mice. Moreover, it is worth noting that the dysregulation of Shh signal transduction largely anticipated the proliferation defect of GN precursors, as indicated by the finding that abnormal transcript levels were already observed in Npc1-deficient cerebella of PN7 mice (Supplementary Material, Fig. S1).

To better characterize Ptch and Smo expression, we also performed western blot analyses in Npc1-deficient mice of increasing ages (PN12, PN18 and PN45). A comparison of Ptch and Smo proteins between cerebella of *wt* and untreated or CD-treated Npc1-deficient mice is shown in Figure 2. This analysis confirmed the significant reduction in Ptch and Smo proteins of Npc1-deficient mice, already observed in transcript levels, except that a significant reduction of Ptch protein appeared from PN18 onward, but not at PN12. The administration of CD re-established in the Npc1-deficient mice, protein levels similar to those of *wt* ones.

Downloaded from https://academic.oup.com/hmg/article/26/12/2277/3098490 by U.S. Department of Justice user on 17 August 2022

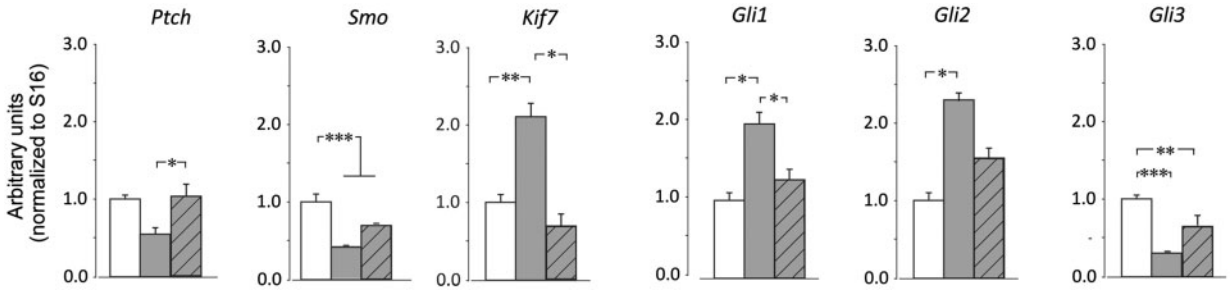

Figure 1. Altered expression of Shh downstream effectors in *Npc1*$^{-/-}$ mice. Transcript levels were determined by semi-quantitative real-time PCR of total RNA of PN12 *wt* (empty bars), *Npc1*$^{-/-}$ (full bars) and *Npc1*$^{-/-}$ CD (dashed bars) mice. Histograms indicate the mean ± S.E.M. of values obtained in three independent assays. Asterisks indicate statistically significant differences (*$P < 0.05$; **$P < 0.01$; ***$P < 0.001$).

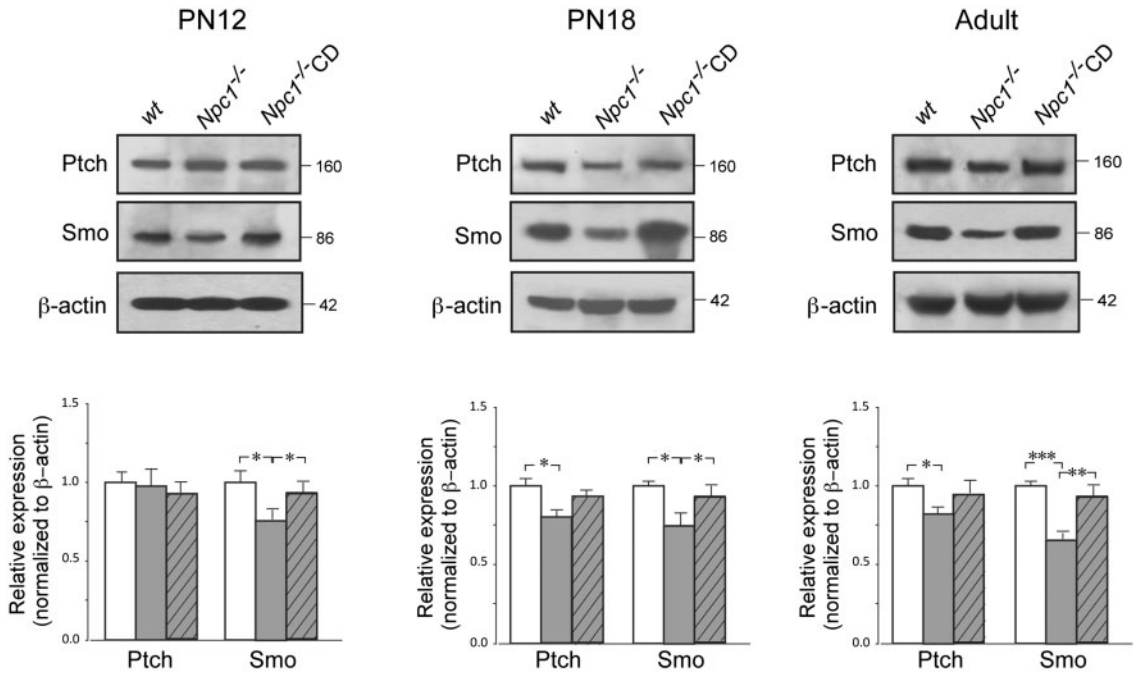

Figure 2. The expression of Ptch and Smo is downregulated in Npc1-deficient cerebella. Western blot analysis of Ptch and Smo protein expression in the cerebella of PN12, PN18 and adult *wt* (empty bars), *Npc1*$^{-/-}$ (full bars) and *Npc1*$^{-/-}$ CD (dashed bars) mice. Histograms indicate the abundance (mean ± S.E.M.) of each protein determined by densitometry of protein bands obtained in three independent experiments, taking β-actin as internal reference. Asterisks indicate statistically significant differences (*$P < 0.05$; **$P < 0.01$; ***$P < 0.001$).

The subcellular localization of Ptch and Smo is severely impaired in Npc1-deficient cerebella

A recent study reported that Ptch and Smo localize at the level of the growth cone and within processes of cerebellar neurons during postnatal development, whereas in PCs, granule neurons and interneurons of the adult cerebellum they predominantly localize at the postsynaptic site (41). We investigated this issue by immuno-electron microscopy, observing a Ptch and Smo subcellular localization in *wt* mouse cerebella that is in agreement with previous observations (41). Protein abundance and subcellular localization, however, were profoundly altered in Npc1-deficient mice (Fig. 3). Specifically, in untreated or CD-treated PN18 *wt* mice, Ptch (Fig. 3C and D) and Smo (Fig. 3H and K) immunopositive vesicles were associated with postsynaptic densities within dendritic spines of PCs. Sometimes, postsynaptic densities themselves appeared positive (Fig. 3C and D, Ptch; 3K, Smo). Both factors, however, were frequently found in vesicular elements within small and large dendritic spines (Fig. 3E, Ptch; 3J and L, Smo), as also associated with their plasma membrane (Fig. 3F, Ptch; 3J, Smo), independently of the presence of an established synapse. Moreover, frequent immunopositive membrane pits and vesicles were seen approaching (or coming from) the spine plasma membranes (Fig. 3B, Ptch; 3L, Smo). Large immunopositive vesicles were also observed within the PC soma, often close to the sites of protein synthesis and maturation (endoplasmic reticulum (rer) and Golgi) (Fig, 3A, Ptch; 3I, Smo). Less frequently, both Ptch and Smo immunopositive vesicles were also clustered in pre-synaptic boutons that granule cells form on PC dendrites, distributed both among synaptic vesicles and very close to the active sites (Fig. 3A and G, Ptch). The presence of Ptch and Smo immunopositive vesicles recycled from the plasma membrane and clustered in multivesicular bodies (mvb) (degradation sites) was the most striking feature characterizing PCs of Npc1-deficient mice (Fig. 3N, Ptch; 3U, Smo). Ptch and Smo immunopositive small vesicles within pre-synaptic boutons (Fig. 3P and Q, Ptch; 3W, Smo), PC soma (Fig. 3M, Ptch) and dendrites (Fig. 3O, Ptch; 3V, Smo) were also

Downloaded from https://academic.oup.com/hmg/article/26/12/2277/3098490 by U.S. Department of Justice user on 17 August 2022

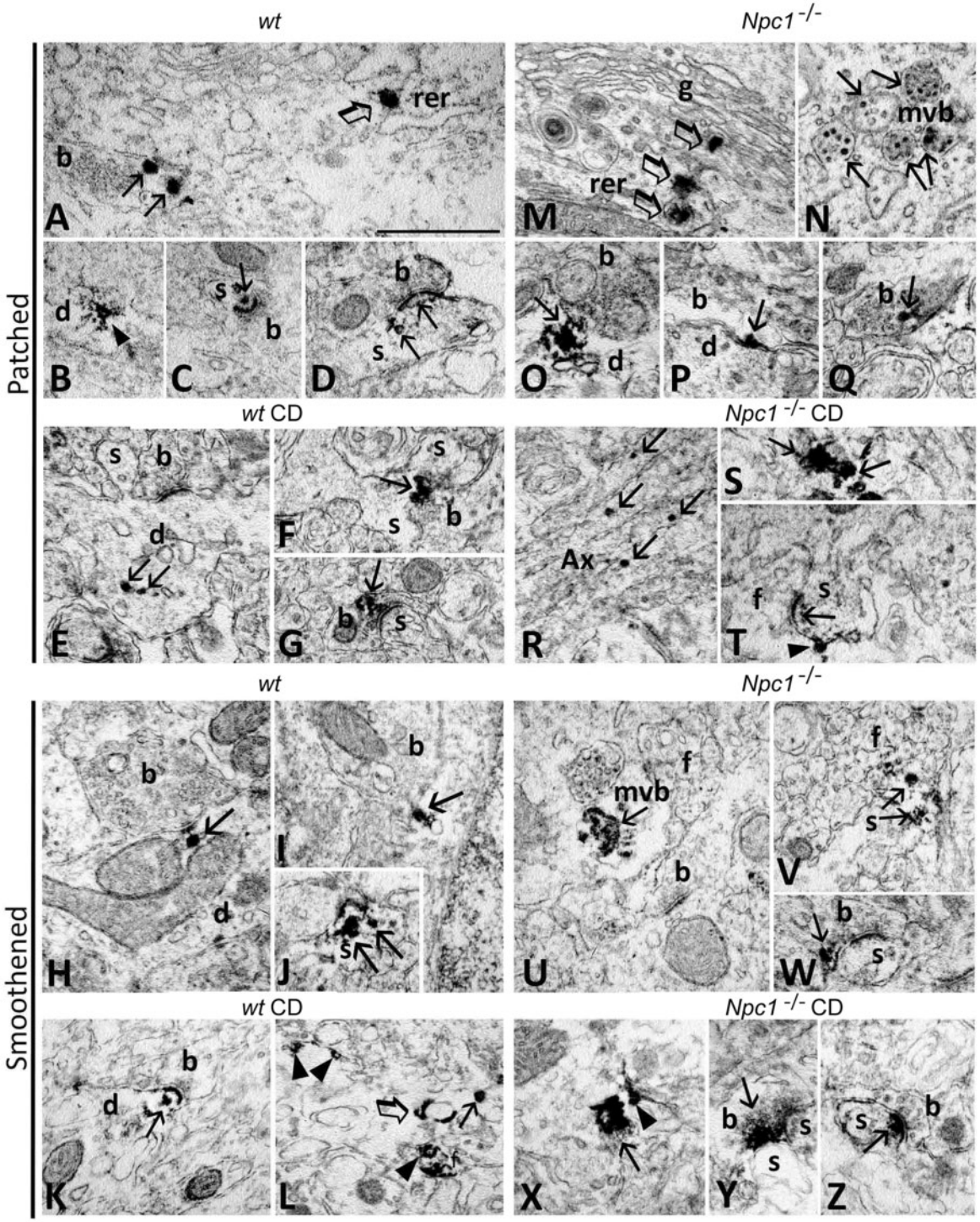

Figure 3. The subcellular distribution of Ptch and Smo is severely impaired in PN18 Npc1-deficient mouse cerebellum compared with *wt*, and recovers after CD treatment. *Anti-patched in wt mice without CD treatment* **(A–D)**. (A) Two large immunopositive vesicles (arrows) are localized within a pre-synaptic bouton approaching a PC soma. Within the cell, a large immunopositive vesicle (open block arrow) is associated with a cistern of the rer). (B) Immunopositive plasma membrane pit (arrowhead) within a dendrite. (C) Immunopositive vesicle (arrow) very close to an immunolabeled post-synaptic density in a dendritic spine. (D) Immunopositivity associated with a postsynaptic density within a dendritic spine facing a pre-synaptic bouton. *Anti-patched in wt mice after CD treatment* **(E–G)**. Amount and localization of patched immunoreactivity does not vary after CD treatment compared with untreated animals. (E) Immunopositive vesicles (arrows) within a terminal dendrite of a PC. (F) Large cluster of immunoreactivity (arrow) in between two dendritic spines and a synaptic bouton. (G) Immunopositive vesicles (arrow) within a pre-synaptic bouton contacting a dendritic spine. *Anti-smoothened in wt mice without CD treatment* **(H–J)**. (H) Large and heavily immunopositive vesicles (arrows) are in the proximity of a post-synaptic specialization within a PC dendrite, flanked by synaptic boutons; (I) in the cell body of a PC, proximal to the plasma membrane, (J) in a dendritic spine. The plasma membrane of the spine is also decorated by immunoreactivity. *Anti-smoothened in wt mice after CD treatment* **(K** and **L)**. Amount and localization of immunoreactivity does not vary after CD treatment compared with untreated animals. (K) An immunopositive vesicle (arrow) in a dendritic spine is localized in the proximity of a post-synaptic density, also immunopositive. (L) Immunopositive vesicle (arrow) localized within a dendrite, which in turn bears immunolabeled plasma membrane pits (upper left

Downloaded from https://academic.oup.com/hmg/article/26/12/2277/3098490 by U.S. Department of Justice user on 17 August 2022

observed. However, the occurrence of immunopositive elements was dramatically less compared with that observed in *wt* mouse specimens, a reduction that was particularly pronounced for Smo. A similar pattern of subcellular distribution of Ptch and Smo immunopositive elements was also observed in PN45 *wt* and Npc1-deficient mice (Supplementary Material, Fig. S2), with the difference that immunopositivity in adult null mice was even more scanty than that observed in CD-untreated PN18 null mice. Moreover, Npc1-null adult mouse cerebella showed consistent neurodegeneration (Supplementary Material, Fig. S2). Conversely, PN18 and PN45 Npc1-null mice that had received the CD treatment recovered Ptch and Smo immunopositivity, the pattern and intensity of which were similar to those of age-matched *wt* mice. This indicates that the re-wiring of the Shh signal transduction is among the molecular mechanisms underlining the CD beneficial effect on rescuing the anomalies of cerebellar morphology (12).

The expression of markers of primary cilium shaft is significantly reduced in Npc1-deficient mouse cerebella

Abnormal patterns of expression and subcellular localization of Ptch and Smo indicate that, besides a reduced level of Shh ligand availability, Npc1-deficiency leads to a widespread disorganization of the machinery involved in Shh signal reception and transduction. In light of the finding that molecular components of this machinery localize at the primary cilium, we asked whether defective primary cilia are responsible for abnormal cerebellum morphogenesis and Shh signaling. To address this question we analyzed the expression levels of ACIII and γ-tubulin, two well-established markers of the cilium shaft and basal body (42,43), respectively. The comparison of protein extracted from *wt* and either untreated or treated Npc1-deficient mice of increasing ages (PN12, PN18 and PN45) showed a significant reduction in both markers at all PN ages, suggesting defective ciliogenesis (Fig. 4). To verify this possibility we sought to visualize primary cilia by immunofluorescence (IF) and/or immunohistochemistry (IHC) on histological sections of *wt* and Npc1-deficient mouse cerebella. Unfortunately, this analysis was extremely challenging due to the tight packaging of the granule neurons of both the external and internal layers of PN12 and adult cerebella, although scanty and stubby primary cilia could be visualized (Supplementary Material, Fig. S3). Meanwhile, we also noticed that the detection and identification of primary cilium at the level of hippocampus was easier (Supplementary Material, Fig. S4), likely because hippocampal neurons mostly complete their differentiation prior to birth (44). Conversely, neurons of the postnatal cerebellum are still differentiating at PN12 and thus display a highly variable primary cilium presence, position and length, as differentiating neurons do (45).

Primary cilia of Npc1-deficient neurons and NPC1 patient fibroblasts display a reduced length

Our analysis of primary cilium morphology in hippocampal sections showed that adult hippocampal cells of both dentate gyrus and cornus ammonis had longer cilia as compared with PN12, in agreement with previous studies (46,47). Based on this observation, and in light of the similarities between cerebellum and hippocampus with respect to the expression of Shh signaling components (48), we thought it was reasonable to perform morphological analyses of cilia on sagittal sections of adult hippocampus. We therefore analyzed the fraction of ciliated cells and the length of primary cilia on the hippocampus of adult *wt* mice and compared them to those of either untreated or CD-treated Npc1-deficient mice. Primary cilia were routinely detected with antibodies directed to ACIII. This analysis showed that the fraction of hippocampal neurons provided with cilia was significantly reduced in Npc1-deficient hippocampi compared with the *wt* ones (Fig. 5A and B). Strikingly, the cilia of Npc1-deficient neurons also displayed a 25% length reduction with respect to *wt*. The treatment with CD led neurons of Npc1-deficient mice to display a fraction of ciliated cells and cilium length similar to those of *wt* mice (Fig. 5B and C), indicating that defective ciliogenesis was rescued by the CD administration. In contrast, CD administration had no effect on the neurons of *wt* mice (Fig. 5A–C).

Besides neurons, fibroblasts represent a convenient model system for studying ciliogenesis, as they respond to Shh stimulation, even though they do not release the Shh ligand (49). We therefore took advantage of NPC1 human fibroblasts to determine whether the defective ciliogenesis observed in neurons of Npc1-deficient mice was also a feature of the disease in humans. To this aim, we first performed co-IF analyses on *wt* and NPC1 human fibroblasts of acetylated α-tubulin that binds microtubules and thus allows the visualization of the primary cilium axoneme, and γ-tubulin, a specific marker of the basal body. Consistent with our findings in the mouse model, both the fraction of NPC1 human fibroblasts provided with cilia and the cilium length was significantly reduced when compared with fibroblasts from healthy controls (Fig. 6A). In light of these findings, we next assessed the effect of CD on cilium length in human fibroblasts. To this end, the culture medium of control and NPC1 fibroblasts was supplemented with increasing concentrations of CD and the cilium length was determined by IF.

arrowheads) and intracellular membrane profiles (open block arrow). Another large immunopositive pit (lower right arrowhead) is observed in the nerve fiber running close by. *Anti-patched in Npc1-deficient mice without CD treatment* **(M–Q)**. (M) Large immunopositive vesicles (open arrowheads) are moving from cisterns of the rer to the Golgi apparatus (g). (N) A cluster of mvb contain immunopositive vesicles (arrows) recycled from the plasma membrane. (O) Very large aggregate of immunoreactivity localized near to the post-synaptic membrane of a PC dendrite. (P) Immunopositive small vesicles (arrow) tightly juxtapose to the plasma membrane of a synaptic bouton. (Q) Immunopositive vesicle (arrow) within a pre-synaptic bouton. *Anti-patched in Npc1-deficient mice after CD treatment* **(R–T)**. Amount, intensity, size and localization of the immunoprecipitates increase after CD treatment compared with untreated animals. (R) Large, single immunopositive vesicles (arrows) travel along adjacent parallel fibers (Ax). (S) Large vesicular aggregates of immunoreactivity (arrows) localized in the soma of a PC. (T) Immunoreactivity (arrow) decorates a portion of the plasma membrane of a dendritic spine and fills an invaginating plasma membrane pit (arrowhead) in the adjacent nerve fiber (f). *Anti-smoothened in Npc1-deficient mice without CD treatment* **(U–W)**. (U) Immunopositive (arrow) mvb within a PC soma. Close by, another mvb is immunonegative. (V) Immunopositive vesicles (arrows) within a dendritic spine. f, nerve fibers. (W) Small immunopositive vesicles (arrow) localized close to the pre-synaptic membrane of a bouton. *Anti-smoothened in Npc1-deficient mice after CD treatment* **(X–Z)**. Amount, intensity, size and localization of the immunoprecipitates increase after CD treatment compared with untreated animals. (X) A large aggregate of immunoreactivity, clustered around a vesicular structure (arrow), is localized within a PC soma. Close by, an immunopositive vesicle (arrowhead) is associated with the plasma membrane. (Y) Immunopositive vesicles (arrow), clustered in a synaptic bouton, are tightly juxtaposed to the pre-synaptic plasma membrane. (Z) Intense aggregates of immunoreactivity are associated with a post-synaptic density in a dendritic spine. Common abbreviation: d, dendrites; s, dendritic spines; b, presynaptic boutons. Scale bar: 1 μm.

Downloaded from https://academic.oup.com/hmg/article/26/12/2277/3098490 by U.S. Department of Justice user on 17 August 2022

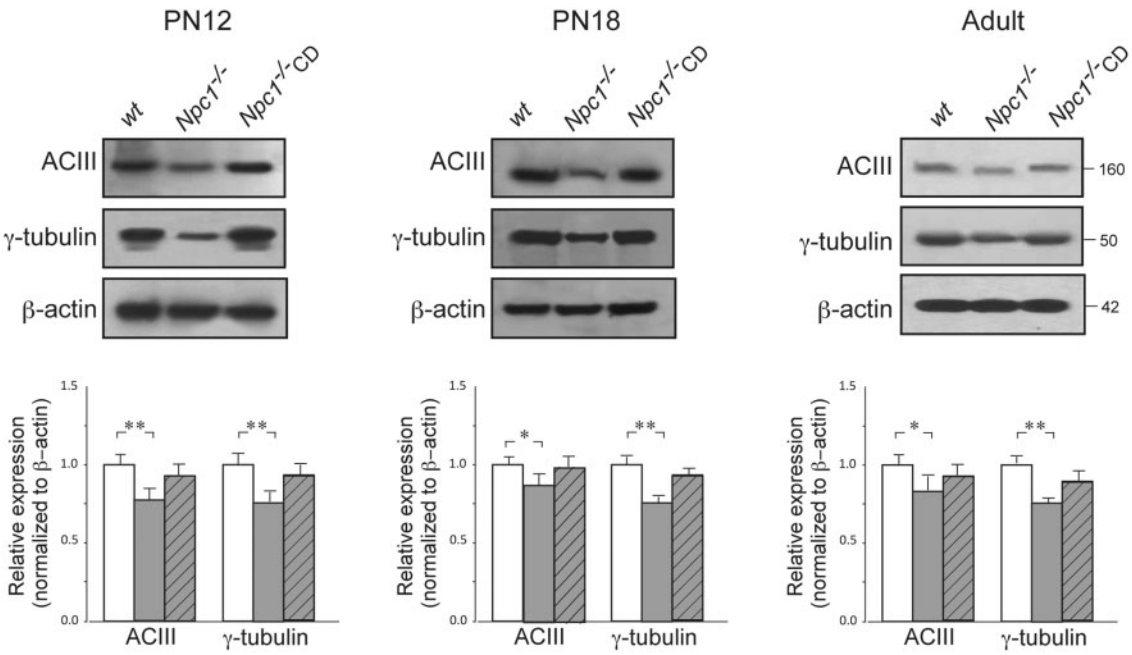

Figure 4. The expression of primary cilium shaft markers is significantly reduced in Npc1-deficient mouse cerebella. Western blot analysis of primary cilium markers, ACIII and γ-tubulin, in cerebella of PN12, PN18 and adult *wt* (empty bars), *Npc1*$^{-/-}$ (full bars) and *Npc1*$^{-/-}$ CD (dashed bars) mice. Histograms indicate the abundance (mean ± S.E.M.) of each protein determined by densitometry of protein bands obtained in three independent experiments, taking β-actin as internal reference. Asterisks indicate statistically significant differences (*$P < 0.05$; **$P < 0.01$).

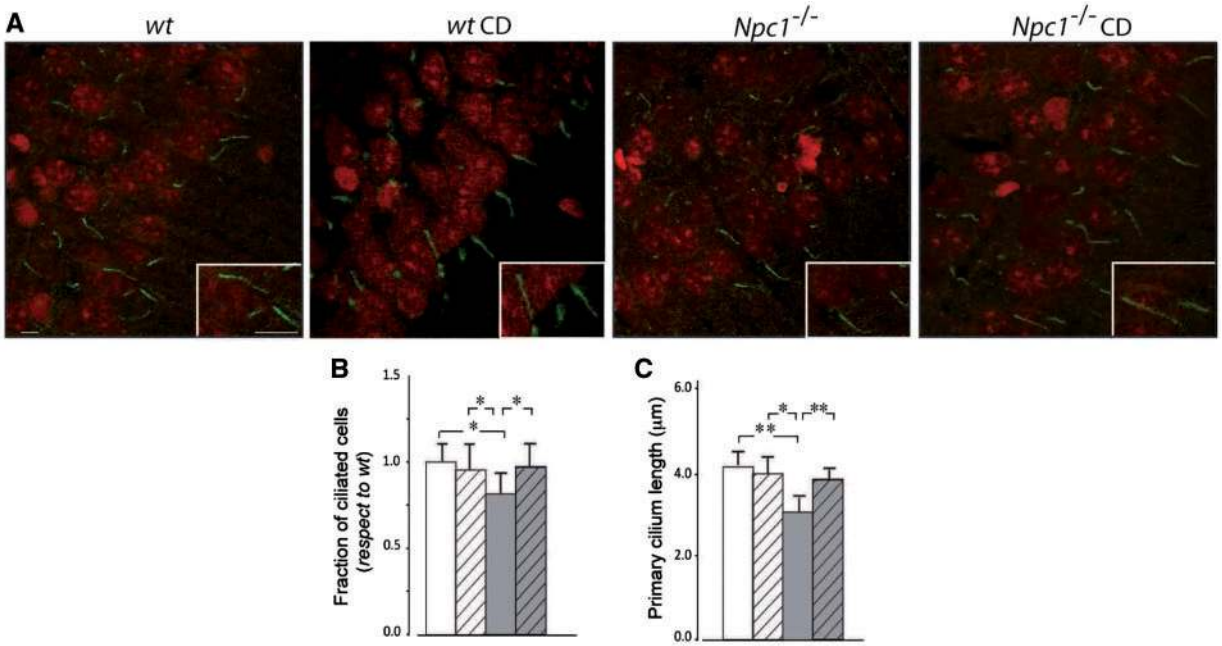

Figure 5. Primary cilia of Npc1-deficient neurons display a reduced length. **(A)** Detection of primary cilia of the hippocampus of adult *wt* and *Npc1*$^{-/-}$ mouse, either untreated or CD-treated, by IF with antibodies against ACIII (green). Representative fields of confocal images are shown in the figure. Scale bar: 2.5 μm. Nuclei were stained with propidium iodide (red). Insets (bottom right) higher magnifications. Scale bar: 5 μm. **(B, C)** Histograms indicate (mean ± S.E.M.) the proportion of ciliated cells and the primary cilium length of adult *wt* (empty bars) and *Npc1*$^{-/-}$ (full bars) mouse, either untreated (empty dashed bars) or CD-treated (full dashed bars), determined by examining 800 cells per experimental group. Asterisks indicate statistically significant differences (*$P < 0.05$, **$P < 0.01$).

The exposure of cells to CD resulted in a significant rescue of the cilium length of Npc1-deficient fibroblasts, no CD effect being observed in control fibroblasts (Fig. 6B). In particular, both CD concentrations caused a significant improvement, which was more pronounced with the higher concentration.

Discussion

The findings of this study expand the present knowledge of the molecular and cellular mechanisms that underlie the mild cerebellar hypoplasia of *Npc1*$^{-/-}$ mice (12), by demonstrating that

Downloaded from https://academic.oup.com/hmg/article/26/12/2277/3098490 by U.S. Department of Justice user on 17 August 2022

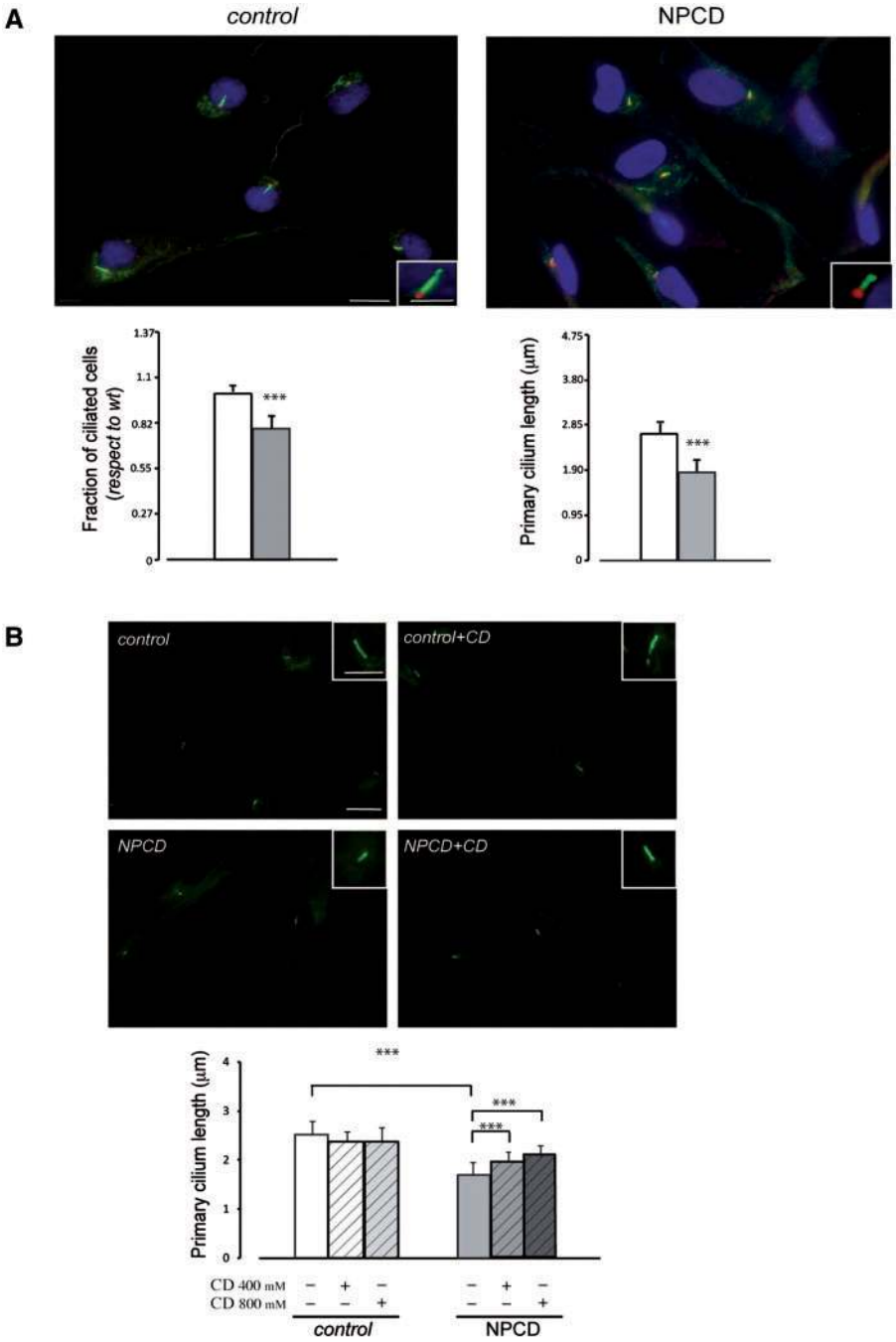

Figure 6. Primary cilia of NPC1 patient fibroblasts display a reduced length. **(A)** Detection of primary cilia of cultured human fibroblasts from healthy control (right) and NPC1 patients (left), by IF with antibodies against acetylated α-tubulin (green) and γ-tubulin (red). Representative fields are shown in the figure. Insets (bottom right), higher magnifications. Nuclei were stained with DAPI. Scale bar: 20 μm (panels) and 5 μm (insets). Histograms indicate (mean ± S.E.M.) the proportion of ciliated cells (right) and the primary cilium length (left) of control (empty bars) and NPC1 patients (full bars) **(B).** Detection of primary cilia of cultured human fibroblasts from healthy control and NPC1 patients cultured for 24 h in the presence of 400 or 800 μM CD and immunostained with antibodies against acetylated α-tubulin (green). Representative fields are shown in the figure. Insets (upper right) higher magnifications. Histograms indicate (mean ± S.E.M.) the proportion of ciliated cells and the primary cilium length of healthy controls ($n = 4$) and NPC1 patients ($n = 7$) determined by examining at least 100 cells per experimental group. Asterisks indicate statistically significant differences (***$P < 0.001$). Scale bar: 20 μm (panels) and 5 μm (insets).

Shh signal generation and reception at the primary cilium are negatively affected by Npc1-deficiency. This conclusion is in agreement with genetic studies in both mouse models and congenital human syndromes that have extensively demonstrated the dependence of normal cerebellar morphogenesis and size on Shh signaling at the level of primary cilium (15,50). In addition, our results emphasize the influence of cholesterol metabolism on the Shh pathway, as already suggested by the finding that the congenital malformations of Smith-Lemli-Opitz syndrome, which is due to mutations in the gene encoding the cholesterol biosynthetic enzyme 7-dehydrocholesterol reductase, are similar to those caused by aberrant Shh signaling (51). More recently, the ablation of 3β-hydroxysterol dehydrogenase, an enzyme involved in one of the later steps of cholesterol

Downloaded from https://academic.oup.com/hmg/article/26/12/2277/3098490 by U.S. Department of Justice user on 17 August 2022

biosynthesis, demonstrated the absolute requirement for cholesterol biosynthesis in the developing CNS after the complete formation of the BBB (34). Because *Npc1* deficiency severely affects granule cell proliferation and Shh signaling is significantly down-regulated, it is likely that the developing cerebellum is very dependent on cholesterol, perhaps attached to Shh (28), as also suggested by the finding that the deficiency for the essential embryonic carrier of cholesterol, apolipoprotein B, particularly affects the hindbrain formation (52).

The addition of fatty acids (53) improves Shh hydrophobicity and localization to lipid rafts which are increased in primary cilia, since ciliary membranes are unusually enriched in sterols, glycolipids and sphingolipids (54). However, the finding of a soluble, diffusible and cholesterol-modified form of Shh in conditioned media, a form which had a gradient in the chick limb, argues against an essential role of the Shh-cholesterol and lipid raft association for Shh signaling (55), although this notion is now heavily discounted (56). Another alteration observed in Niemann-Pick C1 that may be relevant to Shh signaling in primary cilium is the elevated caveolin-1 level (57), since Ptch associates with caveolin-1 in lipid rafts (58). An excess of Ptch is likely to require greater amounts of Shh ligand for inhibition of the repression it exerts on Smo. Moreover, the fact that Ptch contains a sterol-sensing domain (29) and is involved in the efflux of cholesterol from the cell (37), likely contributing to the repression of Smo, also argues for a negative effect of cholesterol dishomeostasis on Shh signaling in NPC1 disease.

Our measurements of mRNA levels of *Shh* pathway components, *Ptch* and *Smo*, and downstream effectors *Gli1-3*, in PN7 and PN12 cerebella, have shown that they are consistently dysregulated in *Npc1*$^{-/-}$ mice. While the down-regulation of *Ptch* and *Smo* transcripts is in agreement with the decreased availability of Shh ligand in Npc1-deficient cerebella (12), the explanation for the changes we observed in the expression levels of *Kif7* and *Gli* factors is quite puzzling. In particular, instead of an increase, we would have expected a reduction of *Gli1* and *Gli2* transcripts, due to their expression being directly regulated by Shh (49). On the other hand, the decrease of *Gli3* mRNA levels in the cerebellum of *Npc1*$^{-/-}$ mice is consistent with the presence of a defective Shh signaling leading to abnormal cerebellar morphogenesis. Gli3, one of 3 Gli downstream effectors of Shh, has both activator and repressor forms. It has been well shown to play a critical role in Shh signaling in the developing cerebellum where it coordinates growth and 3D patterning (59). The level of Gli3^{R} is regulated by Shh to control neural stem cell proliferation (60). Importantly, as suggested by our data, not only is the cerebral cortical size regulated by primary cilia and Gli3 activity (61), but also the cerebellum. The dysregulation of *Gli* transcription factors is possibly linked to a disorganization of the primary cilium tip compartment, as suggested by the abnormal expression of *Kif7* in *Npc1*$^{-/-}$ mice. Kif7, the vertebrate homolog of *Drosophila Costal2*, is a kinesin motor protein belonging to the kinesin-4 family, which regulates the activity of *Cubitus interruptus* (the *Drosophila* homolog of the Gli transcription factors) (62,63). It was recently shown that Kif7-mutant neural progenitors and cultured fibroblasts have abnormally long primary cilia with structural defects at the ciliary axoneme (21). Our data are consistent with the notion that *Kif7* over-expression leads to shorter cilia and decreased *Shh* signaling.

The overall reduction and marked disorganization of Ptch and Smo subcellular localization which we have shown in Npc1-deficient mice by transmission electron microscopy further supports the presence of defective Shh signal reception in our murine model of NPC1 disease. Particularly intriguing is the presence of Ptch and Smo immunopositive vesicles recycling from the plasma membrane and clustered in mvbs (degradation sites) in PCs of *Npc1*$^{-/-}$ mice; this indicates a severe impairment of autocrine Shh signaling in these cells and may explain their selective vulnerability to Npc1-deficiency.

The overall disorganization of Shh signaling, along with the shortening of primary cilia, raises the possibility of considering NPC1 disease a ciliopathy. In fact, recent studies have linked defects of genes encoding for ciliary proteins to various cerebellar disorders (64), laying the basis for a coherent definition and classification of human ciliopathies. These are genetic diseases initially grouped by clinicians on the basis of most striking clinical features (Bardet Biedl syndrome for its polydactyly, obesity and retinitis pigmentosa, now known to be the result of mutations of ~10 different ciliary genes; and Joubert syndrome for its cerebellar dysplasia but now known to be sometimes associated with diverse features, including those of Bardet-Biedl syndrome, with ~15 ciliary protein genes, possibly mutated). The relative severity of the cilia defects can vary from place to place, even within different brain areas (65), likely explaining the different, but partially overlapping, clinical features among ciliopathies. Post-mortem findings in the brain of Joubert syndrome were described as total aplasia of the cerebellar vermis with dysplasia and numerous heterotopias of cerebellar nuclei (66). Such cerebellar dysplasia, along with retinal abnormalities (67) and anosmia, (68) are shared between Niemann-Pick C1 mutants and other ciliopathies. Thus, a good case can be made for classifying the pre-inflammation and neurodegenerative stages of Niemann-Pick C1 as a ciliopathy.

A putative candidate for altered ciliogenesis in NPC1 disease is altered autophagy, although the role of autophagy in NPC1 disease has so far been controversial. Pacheco *et al.* (69) observed increased levels of basal autophagy as indicated by elevated amounts of LC3-II in NPC1 deficient mouse and human fibroblasts cultured in the presence of non-delipidated serum. However, when autophagic flux was measured, instead of just monitoring amounts of LC3-II, impaired degradation and accumulation of autophagosomes was observed (70). These results obtained with cultured fibroblasts were also extended to NPC1 cultured neurons and the autophagic defect was shown to lead to decreased viability of the mutant neurons (71). Such a defect could be caused by the altered ciliogenesis we detected; alternatively, the shortened cilia could be influenced by the altered autophagy, due to primary cilium formation and autophagy being two mutually regulated processes during serum starvation (72). However, these authors also studied the balance between the two processes by blocking the intracellular flagellar transport, suggesting that limitations of these ciliary components by autophagy limits ciliary growth; this suggests that autophagy may be primary. However, it is worth noting that the shortened cilia we have detected in human mutant fibroblasts were found while the cells were well supplied with cholesterol and protein, namely conditions that certainly do not increase autophagy.

The findings of this study are significant because they: (i) correlate the defective Shh signaling to the mild hypoplasia of the cerebellum and; (ii) show for the first time that the formation of the primary cilium is altered in NPC1 disease.

Materials and Methods

Animals and treatments

Npc1$^{-/-}$ mice with BALB/cJ background obtained from heterozygous crosses were exposed to a 12-h light–dark cycle, receiving

Downloaded from https://academic.oup.com/hmg/article/26/12/2277/3098490 by U.S. Department of Justice user on 17 August 2022

Table 1. Genotype of patients included in the study

Patient	Allele 1	Allele 2
NPC1	c.2819C>T (p.S940L)	c.2833G>A (p.D945N)
NPC2	c.3056A>G (p.Y1019C)	c.3056A>G (p.Y1019C)
NPC3	c.710C>T (p.P237L)	c.3304C>T (p.L1102F)
NPC4	c.3182 T >C (p.I1061T)	c.3182 T >C (p.I1061T)
NPC5	c.3424T>C (p.M1142T); c.1943T>A (p.L648H)	c. 298T>A (p.C100S)
NPC6	c.1421 C>T (p.P474L)	c.1501G>T (p.D501Y)
NPC7	c.2291C>T (p.A764V)	c.2819C>T (p.S940L)

All patients presented a classical biochemical phenotype characterized by massive lysosomal accumulation of unesterified cholesterol. The lysosomal accumulation of unesterified cholesterol was demonstrated by filipin staining.

food and water *ad libitum*. Pup genotypes were identified by PCR analysis of tail DNA as described (73). Treatment with CD (Sigma-Aldrich, Milan, Italy) was performed by two subsequent subcutaneous injections of either a 20% solution (w/v; 4000 mg/kg body weight) of CD in phosphate buffered saline (PBS) or plain PBS, for controls, to 4- and 7-day-old mice *Npc1*$^{-/-}$ and *wild-type* (*wt*) littermates (12,74). Experimental protocols and related procedures were approved by the Italian Ministry of Public Health. All efforts were made to minimize animal suffering, according to European Directive 2010/63/EU.

Cell culture and treatments

Human fibroblasts were obtained from skin biopsies from seven patients affected by NPC1 disease, and six healthy controls. All NPC1 disease patients presented the classical biochemical phenotype characterized by massive LE/LY accumulation of unesterified cholesterol in cultured fibroblasts, and diagnosis was confirmed by sequencing both *NPC1* and *NPC2* genes. All patients presented mutations in the *NPC1* gene (Table 1, RefSeq cDNA NM_000271.4). Written consent was obtained from all subjects involved in the study.

Fibroblasts were cultured and maintained in Dulbecco's modified Eagle's medium (Gibco, Paisley, UK) supplemented with 10% fetal calf serum and 50 mg/ml penicillin/streptomycin, in a humidified atmosphere containing 5% CO_2 at 37 °C. To induce primary cilium formation, cells were cultured in a serum-free medium for 24 h in the absence or presence of CD (final concentration of 400 or 800 μM).

Immuno-electron microscopy

PN18 and adult *Npc1*$^{-/-}$ and *wt* mice were deeply anesthetized by an intraperitoneal injection of a mixture of xylazine (20 mg/kg) and ketamine (34 mg/kg) and then transcardially perfused with freshly depolymerized 4% paraformaldehyde (PFA) and 0.05% glutaraldehyde in a 0.1 M phosphate buffer (PB). Cerebella were dissected out, post-fixed in the same fixative overnight (ON) at 4 °C and cut into 50 μm thick sagittal sections using a vibratome. Sections were first cryoprotected in 10% dimethyl sulfoxide (DMSO) + 1% glycerol (10 min at 4 °C) and 20% DMSO + 2% glycerol (2× 10 min at 4 °C), and then frozen-thawed four times in liquid nitrogen-cooled isopentane, for tissue permeabilization. After a brief wash in PB, endogenous peroxidases were blocked by incubation in 10% methanol and 3% H_2O_2 in 0.1 M PB (10 min at RT). Sections were rinsed again, incubated in a blocking solution (1% bovine serum albumin, BSA, 10% normal goat serum, NGS, in 0.1 M PB) for 1 h at RT and then in the primary antibodies, rabbit anti-Ptch and rabbit anti-Smo, diluted in 1% BSA, 1% NGS in 0.1 M PB (Table 2).

After a rinse in PB, sections were incubated with the appropriate secondary antibody (Table 2) for 1 h at RT. Antibody binding sites were revealed for 10 min in 0.05% 3,3′-diaminobenzidine and 0.1% H_2O_2 in 0.1 M PB. After a thorough wash in PB, sections were post-fixed in 1% osmium tetroxide (1 h at 4 °C), rinsed in bi-distilled chilled water (1 h) and 50% ethyl alcohol (5 min), en-block stained for 20 min in 1% uranyle acetate in 70% ethyl alcohol, and dehydrated in a series of ascending ethyl alcohol and propylene oxide. After an ON incubation in a mixture 1:1 of propylene oxide: Epon epoxy resin (Fluka; Sigma-Aldrich), and 4 h in Epon, samples were flat embedded and polymerized for 3 days at 60 °C. Ultra thin sections were cut both tangential and orthogonal to the embedded vibratome sections, collected on copper grids, counterstained with a 0.2% lead citrate aqueous solution and viewed at a Philips EM208S electron microscope connected to a Megaview III video camera. Acquired images were adjusted for light and contrast with the Adobe Photoshop CS6 software.

Light microscopy histology, immunohistochemistry and immunofluorescence

Npc1$^{+/+}$ (*wt*) and *Npc1*$^{-/-}$ mice of postnatal days 12 (PN12), 18 (PN18) and 45 (adult) (4 mice/genotype/age), treated or not with CD, were anaesthetized, as described above, and then transcardially perfused with freshly depolymerized 4% PFA in 0.1 M PBS. Brains were then further fixed in 4% PFA ON at 4 °C, cryoprotected with sucrose (30% in PBS), embedded in FSC22 Clear R Frozen Section Compound (Leica Biosystems, Milan, Italy) and serially sectioned (slice thickness 25 μm) using a Leica CM 1900 cryostat. Sagittal sections were placed in PBS, separated into individual wells of a 24-well plate. Free floating sections were then permeabilized with 0.3% Triton X-100 in PBS supplemented with 2% NGS and 10 mg/ml BSA (Sigma-Aldrich). All incubations and washes were carried out in PBS. Sections were incubated with antibodies against the ciliary marker Adenylate cyclase III (ACIII) (Santa Cruz Biotechnologies; or ProteinTech Group, Milan, Italy) (Table 2) ON at 4 °C and processed for IHC or IF.

In IHC assays, staining was revealed by using the rabbit Vectastain Elite ABC kit (Vector Laboratories Inc., Burlingame, CA, USA) and peroxidase substrate Vector VIP (Vector Laboratories Inc.), according to the manufacturer's instructions. IF assays were performed using free-floating brain sections and cultured human fibroblasts. After the incubation with the primary antibody, brain sections were washed three times in PBS and incubated with Alexa Fluor 488- or 555-conjugated secondary antibodies (Invitrogen, Milan, Italy) (Table 2) for 1 h at RT.

Downloaded from https://academic.oup.com/hmg/article/26/12/2277/3098490 by U.S. Department of Justice user on 17 August 2022

Table 2. Antibodies used

Antibody		Company	Dilution	
			WB[a]	IHC/IF/TEM[b]
Primary	anti-γ-tubulin	Sigma Aldrich; no.T5192	1:2000	1:500
	anti-γ-tubulin	Sigma Aldrich; no.T6557	1:10000	1:5000
	anti-acetylated tubulin	Sigma Aldrich; no.T6793	1:6000	1:1500
	anti-ACIII (C-20)	Santa Cruz; sc-588	1:200	1:100
	anti-ACIII	ProteinTech Group Inc; no.19492-1-AP	1:1000	1:50
	anti-GAPDH	Sigma Aldrich; no.G9545	1:10 000	—
	anti-patched	AbCam; no.Ab53715	1:500	1:1000
	anti-smoothened	AbCam; no.Ab38686	1:250	1:500
	anti-β-actin	AbCam; no.ab6276	1:5000	—
Antibody		Company	Dilution	
			WB[a]	IHC/IF/TEM[b]
Secondary	Horseradish peroxidase-conjugated goat anti-rabbit IgG	Thermo Fisher Scientific; no.32460	1:200	—
	Horseradish peroxidase-conjugated goat anti-mouse IgG	Thermo Fisher Scientific; no.32430	1:650	—
	Biotinylated goat anti-rabbit IgG	Vector Laboratories, Burlingame; no.PK-6101	—	1:200
	Biotinylated goat anti-mouse IgG	Vector Laboratories; no.PK-6102	—	1:200
	Goat anti rabbit IgG	Covance; no.SMI-5030C		1:400
	Activity-select PA anti-rabbit	Covance; no.SMI-4010L	—	1:100
	Alexa Fluor 488 conjugated goat anti-rabbit	Thermo Fisher Scientific; no.A-11008	—	1:500
	Alexa Fluor 488 conjugated goat anti-mouse	Thermo Fisher Scientific; no.A-21422	—	1:500

[a]WB, western blot assay.

[b]IHC, immunohistochemistry; TEM, transmission electron microscopy.

Nuclei were stained with Hoechst 33258 (Sigma-Aldrich). Sections were transferred on glass slides and mounted by using the Vectashield Mountain Medium (Vector Laboratories). Human fibroblasts, grown on glass cover slips, were fixed with 4% PFA, permeabilized with an ice-cold solution of methanol/acetone (1:1) for 10 min at −20 °C and blocked in 2% BSA in PBS. Cells were then incubated ON at 4 °C with the primary antibodies directed against acetylated alpha-tubulin (Sigma-Aldrich) and γ-tubulin (Sigma-Aldrich) and thereafter with the appropriate Alexa Fluor 555- or 488-labeled secondary antibodies (Life Technologies, Invitrogen, Milan, Italy), for 1 h at 37 °C. Cover slips were mounted with the DAPI-containing VECTASHIELD Mounting Medium (Vector Laboratories). Immunodetection specificity was assessed by omitting the primary antibody in IHC and IF assays. A list of primary and secondary antibodies used is provided in Table 2.

Measurements of primary cilia

Imaging and quantification of the fraction of ciliated cells and cilium length was performed using a Leica TCS NT confocal laser (Leica Microsystem) with a 40× and 100× immersion objective lens and ×4 optical zoom, a Leica DMI 6000B microscope connected to a Leica DFC350FX camera (Leica Microsystems) and a Zeiss Axioplan microscope. Due to the differences in the z resolution of the confocal microscope, compared with the x and y planes, only cilia that were ∼90° to the incident light were selected. Serial optical z-sections were collected for each image. Two-dimensional projections of cilia were acquired from a minimum of 30 cells for each area (CA1 of hippocampus) and cilium length was measured using the 'z projection' function of Image J NIH software (NIH Image, Bethesda, MD). When the length of cilia was determined by using optical microscopes, the cover slips were pressed hard against microscope slides to flatten most of the cilia. Only cilia that were flattened into one plane were selected for image acquisition and cilium length measurement (75). The distance from the base to the tip of the cilium was measured by tracing the length of the cilium, using Image J's segmented line tool (rsb.info.nih.gov/ij). The fraction of ciliated cells in a given field was determined by counting the number of cilia and the number of nuclei and expressed as a % of total cells. Cilia prevalence was measured in 10 fields (almost 25 cells/field) in three separate experiments, giving a total of 800 mouse cells and 100 human fibroblasts respectively per experimental group.

RNA preparation and real-time RT-PCR

Total RNA was extracted from cerebella of PN7-PN12, *wt* and *Npc1*$^{-/-}$ mice, treated or not with CD, using the RNeasy Lipid Tissue mini kit (Qiagen, Hilden, Germania). cDNA was synthesized using the NZY First-Strand cDNA Synthesis kit (NZYtech, Campus do Lumiar, Lisboa), following the protocol supplied by the manufacturer. Real-time RT-PCR was performed by using the KAPA SYBR qPCR kit (Kapa Biosystems, Boston, USA) with the following cycling conditions: 95 °C for 10 min, then 35 cycles at 95 °C for 10 s and 62 °C for combined annealing/extension for 30 s. The QuantiFast PCR primers were: Mm_Ptch_SG (Cat No. QT00149135), Mm_Gli1_SG (Cat No. QT00173537), Mm_Gli2_SG (Cat No. QT00291711), Mm_Gli3_SG (Cat No. QT00102256) and Mm_Rps16_SG (Cat No. QT0009256) (S16 ribosomal protein); Mm_Smo_F: GCTGCCACTTCTATGACTTCT R: GCCGATTCTTGA TCTCACAGT; Mm_Kif7_F: CTGGAGAAGGAACTAGGTCG R:TTT CCAGGCAGAGGCTTCTC. Gene expression levels between experimental groups were analyzed using the 2ΔΔCt method (76). cDNA amounts were normalized to Rps16 and expressed as the fold-increase over control. Expression levels were also normalized to *Gapdh* (not shown).

Downloaded from https://academic.oup.com/hmg/article/26/12/2277/3098490 by U.S. Department of Justice user on 17 August 2022

Western blot analysis

For western blot analyses, total protein from PN12, PN18 and PN45 *Npc1*$^{-/-}$ and *wt* littermate cerebella (four mice/genotype/age) were extracted with RIPA buffer (Sigma-Aldrich) supplemented with protease and phosphatase inhibitors (Roche Life Science Indianapolis, IN, USA), as previously described in (77). Protein concentration was routinely determined by Bradford's colorimetric assay (Bio-Rad, Milan, IT). Equal amounts of total protein/lane were fractionated by electrophoresis on a 4-12% gradient SDS-polyacrylamide gel (Bolt Bis-Tris Plus gels, Life Technologies) or 10% gel pre-cast (Bio-Rad). Fractionated proteins were transferred to PVDF membranes (GE Healthcare, Little Chalfont, UK) and, after blocking, membranes were incubated ON at 4°C with the primary antibodies, washed, incubated with the appropriate secondary antibody for 1 h at RT and developed with the SuperSignal West Dura reagent (Thermo Scientific/Pierce, Rockford, IL, USA). The primary and secondary antibodies used are reported in Table 2. Immunopositive bands were quantified by using a Gel Doc 2000 videodensitometer (Biorad, Hercules, CA, USA).

Statistics

Statistical analyses were performed using the GraphPad Prism version 5.0d (GraphPad, La Jolla, CA). Data is expressed as mean values ± SEM. Statistically significant differences were analyzed by one- and two-way ANOVA and Tukey *post hoc* tests. *P*-values <0.05 were considered significant. The unpaired student's *t*-test was used to evaluate differences between *wt and* *Npc1*$^{-/-}$ at PN7.

Supplementary Material

Supplementary Material is available at *HMG* online.

Acknowledgements

We are grateful to Carla Battisti for technical advice for the detection of the primary cilium of human fibroblasts.

Conflict of Interest statement. None declared.

Funding

This work was supported by Telethon Foundation, Italy (grant no. GGP13183) and Ateneo La Sapienza (grant no C26V127RC3) to M.T.F.

References

1. Sleat, D.E., Wiseman, J.A., El-Banna, M., Price, S.M., Verot, L., Shen, M.M., Tint, G.S., Vanier, M.T., Walkley, S.U. and Lobel, P. (2004) Genetic evidence for non-redundant functional cooperativity between NPC1 and NPC2 in lipid transport. *Proc. Natl. Acad. Sci. USA*, **101**, 5886–5891.
2. Infante, R.E., Wang, M.L., Radhakrishnan, A., Kwon, H.J., Brown, M.S. and Goldstein, J.L. (2008) NPC2 facilitates bidirectional transfer of cholesterol between NPC1 and lipid bilayers, a step in cholesterol egress from lysosomes. *Proc. Natl. Acad. Sci. USA*, **105**, 15287–15292.
3. Kwon, H.J., Abi-Mosleh, L., Wang, M.L., Deisenhofer, J., Goldstein, J.L., Brown, M.S. and Infante, R.E. (2009) Structure of N-terminal domain of NPC1 reveals distinct subdomains for binding and transfer of cholesterol. *Cell*, **137**, 1213–1224.
4. Deffieu, M.S. and Pfeffer, S.R. (2011) Niemann–Pick type C function requires luminal domain residues that mediate cholesterol-dependent NPC2 binding. *Proc. Natl. Acad. Sci. USA*, **108**, 18932–18936.
5. Vincent, I., Bu, B. and Erickson, R.P. (2003) Understanding Niemann-Pick type C disease: A fat problem. *Curr. Opin. Neurol.*, **16**, 155–161.
6. Vanier, M.T. (2010) Niemann-Pick type C disease. *Orphanet J. Rare Dis.*, **5**, 416.
7. Borbon, I., Totenhagen, J., Fiorenza, M.T., Canterini, S., Ke, W., Trouard, T. and Erickson, R.P. (2012) Niemann–Pick C1 mice, a model of "juvenile Alzheimer's disease", with normal gene expression in neurons and fibrillary astrocytes show long term survival and delayed neurodegeneration. *J. Alzheimers Dis.*, **30**, 875–887.
8. Fiorenza, M.T., Dardis, A., Canterini, S. and Erickson, R.P. (2013) Cholesterol metabolism-associated molecules in late onset Alzheimer's disease. *J. Biol. Regul. Homeost. Agents*, **27**, 23–35.
9. Dardis, A., Zampieri, S., Canterini, S., Newell, K.L., Stuani, C., Murrell, J.R., Ghetti, B., Fiorenza, M.T., Bembi, B. and Buratti, E. (2016) Altered localization and functionality of TAR DNA Binding Protein 43 (TDP-43) in Niemann- Pick disease type C. *Acta Neuropathol. Commun.*, **4**, 52.
10. Camargo, F., Erickson, R.P., Garver, W.S., Hossain, G.S., Carbone, P.N., Heidenreich, R.A. and Blanchard, J. (2001) Cyclodextrins in the treatments of a mouse model of Niemann-Pick C disease. *Life Sci.*, **70**, 131–142.
11. Liu, B., Turley, S.D., Burn, S., Miller, A.M., Repa, J.J. and Dietschy, J.M. (2009) Reversal of defective lysosomal transport in NPC disease ameliorates liver dysfunction and neurodegeneration in the Npc1−/− mouse. *Proc. Natl. Acad. Sci. USA*, **106**, 2377–2382.
12. Nusca, S., Canterini, S., Palladino, G., Bruno, F., Mangia, F., Erickson, R.P. and Fiorenza, M.T. (2014) A marked paucity of granule cells in the developing cerebellum of the *Npc1*$^{-/-}$ mouse is corrected by a single injection of hydroxypropyl-beta-cyclodextrin. *Neurobiol. Dis.*, **70**, 117–126.
13. Caporali, P., Bruno, F., Palladino, G., Dragotto, J., Petrosini, L., Mangia, F., Erickson, R.P., Canterini, S. and Fiorenza, M.T. (2016) Developmental delay in motor skill acquisition in Niemann-Pick C1 mice reveals abnormal cerebellar morphogenesis. *Acta Neuropathol. Commun.*, **1**, 4–94.
14. Dahmane, N., Ruiz, I. and Altaba, A. (1999) Sonic hedgehog regulates the growth and patterning of the cerebellum. *Development*, **126**, 3089–3100.
15. Spassky, N., Han, Y.G., Aguilar, A., Strehl, L., Besse, L., Laclef, C., Ros, M.R., Garcia-Verdugo, J.M. and Alvarez-Buylla, A. (2008) Primary cilia are required for cerebellar development and Shh-dependent expansion of progenitor pool. *Dev. Biol.*, **317**, 246–259.
16. Vaillant, C. and Monard, D. (2009) SHH pathway and cerebellar development. *Cerebellum*, **8**, 291–301.
17. Aguilar, A., Meunier, A., Strehl, L., Martinovic, J., Bonniere, M., Attie-Bitach, T., Encha-Razavi, F. and Spassky, N. (2012) Analysis of human samples reveals impaired SHH-dependent cerebellar development in Joubert syndrome/Meckel syndrome. *Proc. Natl. Acad. Sci. USA*, **109**, 16951–16956.
18. Goetz, S.C. and Anderson, K.V. (2010) The primary cilium: a signalling centre during vertebrate development. *Nat. Rev. Genet.*, **11**, 331–344.

Downloaded from https://academic.oup.com/hmg/article/26/12/2277/3098490 by U.S. Department of Justice user on 17 August 2022

19. Taipale, J., Couper, M.K., Maiti, T. and Beachy, P.A. (2002) Patched acts catalytically to suppress the activity of Smoothened. *Nature*, **418**, 892–897.
20. Yavari, A., Nagaraj, R., Owusu-Ansah, E., Folick, A., Ngo, K., Hillman, T., Call, G., Rohatgi, R., Scott, M.P. and Banerjee, U. (2010) Role of lipid metabolism in Smoothened derepression in Hedgehog signaling. *Dev. Cell*, **19**, 54–65.
21. He, M., Subramanian, R., Bangs, F., Omelchenko, T., Liem, K.F., Jr., Kapoor, T.M. and Anderson, K.V. (2014) The kinesin-4 protein Kif7 regulates mammalian hedgehog signalling by organizing the cilium tip compartment. *Nat. Cell Biol.*, **16**, 663–666.
22. Cheung, H.O., Zhang, X., Ribeiro, A., Mo, R., Makino, S., Puviindran, V., Law, K.K., Briscoe, J. and Hui, C.C. (2009) The kinesin protein Kif7 is a critical regulator of Gli transcription factors in mammalian hedgehog signaling. *Sci. Signal.*, **2**, ra29.
23. Jiang, J. and Hui, C.C. (2008) Hedgehog signaling in development and cancer. *Dev. Cell*, **15**, 801–812.
24. Tuson, M., He, M. and Anderson, K.V. (2011) Protein kinase A acts at the basal body of the primary cilium to prevent Gli2 activation and ventralization of the mouse neural tube. *Development*, **138**, 4921–4930.
25. Huangfu, D. and Anderson, K.V. (2006) Signaling from Smo to Ci/Gli: conservation and divergence of Hedgehog pathways from Drosophila to vertebrates. *Development*, **133**, 3–14.
26. Ruiz i Altaba, A. (1998) Combinatorial Gli gene function in floor plate and neuronal inductions by Sonic hedgehog. *Development*, **125**, 2203–2212.
27. Haldipur, P., Bharti, U., Govindan, S., Sarkar, C., Iyengar, S., Gressens, P. and Mani, S. (2012) Expression of Sonic hedgehog during cell proliferation in the human cerebellum. *Stem Cells Dev.*, **21**, 1059–1068.
28. Porter, J.A., Young, K.E. and Beachy, P.A. (1996) Cholesterol modification of hedgehog signaling proteins in animal development. *Science*, **274**, 255–258.
29. Carstea, E.D., Morris, J.A., Coleman, K.G., Loftus, S.K., Zhang, D., Cummings, C., Gu, J., Rosenfeld, M.A., Pavan, W.J., Krizman, D.B. *et al.* (1997) Niemann-Pick C1 disease gene: homology to mediators of cholesterol homeostasis. *Science*, **277**, 228–231.
30. Incardona, J.P., Gaffield, W., Lange, Y., Cooney, A., Pentchev, P.G., Liu, S., Watson, J.A., Kapur, R.P. and Roelink, H. (2000) Cyclopamine inhibition of Sonic hedgehog signal transduction is not mediated through effects on cholesterol transport. *Development*, **224**, 440–452.
31. Chiang, C., Litingtung, Y., Lee, E., Young, K.E., Corden, J.L., Westphal, H. and Beachy, P.A. (1996) Cyclopia and defective axial patterning in mice lacking Sonic hedgehog gene function. *Nature*, **383**, 407–413.
32. Nanni, L., Ming, J.E., Bocian, M., Steinhaus, K., Bianchi, D.W., Die-Smulders, C., Giannotti, A., Imaizumi, K., Jones, K.L., Campo, M.D. *et al.* (1999) The mutational spectrum of the Sonic Hedgehog gene in holoprosencephaly: SHH mutations cause a significant proportion of autosomal dominant holoprosencephaly. *Hum. Mol. Genet.*, **8**, 2479–2488.
33. Belloni, E., Muenke, M., Roessler, E., Traverso, G., Siegel-Bartelt, J., Frumkin, A., Mitchell, H.F., Donis-Keller, H., Helms, C., Hing, A.V. *et al.* (1996) Identification of Sonic hedgehog as a candidate gene responsible for holoprosencephaly. *Nat. Genet.*, **14**, 353–356.
34. Cunningham, D., DeBarber, A.D., Bir, N., Binkley, L., Merkens, L.S., Steiner, R.D. and Herman, G.E. (2015) Analysis of hedgehog signalling in cerebellar granule cell precursors in a conditional *Nsdh1* allele demonstrates an essential role for cholesterol in postnatal CNS development. *Hum. Mol. Genet.*, **24**, 2808–2825.
35. Singh, P., Saxena, R., Srinivas, G., Pande, G. and Chattopadhyay, A. (2013) Cholesterol biosynthesis and homeostasis in regulation of the cell cycle. *PLoS One.*, **8**, p. e58833.
36. Incardona, J.P. and Roelink, H. (2000) The role of cholesterol in Shh signaling and teratogen-induced holoprosencephaly. *Cell Mol. Life Sci.*, **57**, 1709–1719.
37. Bidet, M., Joubert, O., Lacombe, B., Ciantar, M., Nehmé, R., Mollat, P., Brétillon, L., Faure, H., Bittman, R., Ruat, M. *et al.* (2011) The hedgehog receptor patched is involved in cholesterol transport. *PLoS One*, **6**, e23834.
38. Dwyer, J.R., Sever, N., Carlson, M., Nelson, S.F., Beachy, P.A. and Parhami, F. (2007) Oxysterols are novel activators of the hedgehog signaling pathway in pluripotent mesenchymal cells. *J. Biol. Chem.*, **282**, 8959–8968.
39. Myers, B.R., Sever, N., Chong, Y.C., Kim, J., Belani, J.D., Rychnovsky, S., Bazan, J.F. and Beachy, P.A. (2013) Hedgehog pathway modulation by multiple lipid binding sites on the smoothened effector of signal response. *Dev. Cell*, **26**, 346–357.
40. Nedelcu, D., Liu, J., Xu, Y., Jao, C. and Salic, A. (2013) Oxysterol binding to the extracellular domain of Smoothened in Hedgehog signaling. *Nat. Chem. Biol.*, **9**, 557–564.
41. Petralia, R.S., Wang, Y.X., Mattson, M.P. and Yao, P.J. (2012) Subcellular distribution of patched and smoothened in the cerebellar neurons. *Cerebellum*, **11**, 972–981.
42. Bishop, G.A., Berbari, N.F., Lewis, J. and Mykytyn, K. (2007) Type III adenylyl cyclase localizes to primary cilia throughout the adult mouse brain. *J. Comp. Neurol.*, **505**, 562–571.
43. Guadiana, S.M., Semple-Rowland, S.L., Daroszewski, D., Madorsky, I., Breunig, J.J., Mykytyn, K. and Sarkisian, M.R. (2013) Arborization of dendrites by developing neocortical neurons is dependent on primary cilia and type 3 adenylyl cyclase. *J. Neurosci.*, **33**, 2626–2638.
44. Supèr, H. and Soriano, E. (1994) The organization of the embryonic and early postnatal murine hippocampus. II. Development of entorhinal, commissural, and septal connections studied with the lipophilic tracer DiI. *Comp. Neurol.*, **344**, 101–120.
45. Lepanto, P., Badano, J.L. and Zolessi, F.R. (2016) Neuron's little helper: The role of primary cilia in neurogenesis. *Neurogenesis*, **3**, e1253363.
46. Arellano, J.I., Guadiana, S.M., Breunig, J.J., Rakic, P. and Sarkisian, M.R. (2012) Development and distribution of neuronal cilia in mouse neocortex. *J. Comp. Neurol.*, **520**, 848–873.
47. Guadiana, S.M., Parker, A.K., Filho, G.F., Sequeira, A., Semple-Rowland, S., Shaw, G., Mandel, R.J., Foster, T.C., Kumar, A. and Sarkisian, M.R. (2016) Type 3 Adenylyl Cyclase and Somatostatin Receptor 3 Expression Persists in Aged Rat Neocortical and Hippocampal Neuronal Cilia. *Front. Aging Neurosci.*, **8**, 127.
48. Petralia, R.S., Schwartz, C.M., Wang, Y.X., Mattson, M.P. and Yao, P.J. (2011) Subcellular localization of Patched and Smoothened, the receptors for Sonic hedgehog signaling, in the hippocampal neuron. *J. Comp. Neurol.*, **519**, 3684–3699.
49. Cohen, M., Kicheva, A., Ribeiro, A., Blassberg, R., Page, K.M., Barnes, C.P. and Briscoe, J. (2015) Ptch1 and Gli regulate Shh signalling dynamics via multiple mechanisms. *Nat. Commun.*, **2**, 6706–6709.

Downloaded from https://academic.oup.com/hmg/article/26/12/2277/3098490 by U.S. Department of Justice user on 17 August 2022

50. Corrales, J.D., Rocco, G.L., Blaess, S., Guo, Q. and Joyner, A.L. (2004) Spatial pattern of Sonic hedgehog signaling through Gli genes during cerebellum development. *Development,* **131**, 5581–5590.
51. Kelley, R.L., Roessler, E., Hennekam, R.C., Feldman, G.L., Kosaki, K., Jones, M.C., Palumbos, J.C. and Muenke, M. (1996) Holoprosencephaly in RSH/Smith-Lemli-Opitz syndrome: does abnormal cholesterol metabolism affect the function of Sonic Hedgehog?. *Am. J. Med. Genet.*, **66**, 478–484.
52. Homanics, G.E., Maeda, N., Traber, M.G., Kayden, H.J., Dehart, D.B. and Sulik, K.K. (1995) Exencephaly and hydrocephaly in mice with targeted modification of the apolipoprotein B (Apob) gene. *Teratology*, **51**, 1–10.
53. Long, J., Tokhunts, R., Old, W.M., Houel, S., Rodriguez-Blanco, J., Singh, S., Schilling, N., Capobianco, A.J., Ahn, N.G. and Robbins, D.J. (2015) Identification of a Family of Fatty-Acid-Speciated Sonic Hedgehog Proteins, Whose members Display Differential Biological Properties. *Cell Rep.*, **10**, 1280–1287.
54. Tyler, K.M., Friedberg, A., Toriello, K.M., Olson, C.L., Cieslak, J.A., Hazlett, T.L. and Engman, D.M. (2009) Flagellar membrane localization via association with lipi rafts. *J. Cell Sci.*, **122**, 859–866.
55. Zeng, X., Goetz, J.A., Suber, L.M., Scott, W.J., Jr, Schreiner, C.M. and Robbins, D.J. (2001) A freely diffusible form of Sonic hedgehog mediates long-range signalling. *Nature*, **411**, 716–720.
56. Ruat, M., Roudaut, H., Ferent, J. and Traiffort, E. (2012) Hedgehog trafficking, cilia and brain functions. *Differentiation*, **83**, 597–604.
57. Garver, W.S., Hsu, S.C.J., Erickson, R.P., Greer, W.L., Byers, D.M. and Heidenreich, R.A. (1997) Increased expression of caveolin-1 in heterozygous Niemann-Pick type II human fibroblasts. *Biochem. Biophys. Res. Commun.*, **236**, 189–193.
58. Karpen, H.E., Bukowski, J.T., Hughes, T., Gratton, J.P., Sessa, W.C. and Gailani, M.R. (2001) The Sonic hedgehog receptor patched associates with caveolin-1 in cholesterol-rich microdomains of the plasma membrane. *J. Biol. Chem.*, **276**, 19503–19511.
59. Blaess, S., Stephen, D. and Joyner, A.L. (2008) Gli3 coordinates three-dimensional patterning and growth of the tectum and cerebellum by integrating Shh and Fgf8 signalling. *Development*, **135**, 2093–2103.
60. Petrova, R., Garcia, A.D.R. and Joyner, A.L. (2013) Titration of GLI3 Repressor activity by Sonic hedgehog signaling is critical for maintaining multiple adult neural stem cell and astrocyte functions. *J. Neurosci.*, **33**, 17490–174905.
61. Wilson, S.L., Wilson, J.P., Wang, C., Wang, B. and McConnell, S.K. (2012) Primary cilia and Gli3 activity regulate cerebral cortical size. *Dev. Neurobiol.*, **72**, 1196–1212.
62. Tay, S.Y., Ingham, P.W. and Roy, S. (2005) A homologue of the Drosophila kinesin-like protein Costal 2 regulates Hedgehog signal transduction in the vertebrate embryo. *Development*, **132**, 626–634.
63. Liem, K.F., He, M., Ocbina, P.J.R. and Anderson, K.V. (2009) Mouse Kif7/Costal2 is a cilia-associated protein that regulates Sonic hedgehog signalling. *Proc. Natl. Acad. Sci. USA*, **106**, 13377–133782.
64. Guemez-Gamboa, A., Coufal, N.G. and Gleeson, J.F. (2014) Primary cilia in the developing and mature brain. *Neuron*, **82**, 511–521.
65. Agassandian, K., Patel, M., Agassandian, M., Storen, K.E., Rahmouni, K., Sheffield, V.C. and Card, J.P. (2014) Ciliopathy is differentially distributed in the brain of a Bardet-Fiedl syndrome mouse model. *PLoS One*, **9**, e93484.
66. Friede, R.L. and Boltshauser, E. (1978) Uncommon syndromes of cerebellar vermis aplasia. I: Joubert syndrome. *Dev. Med. Child Neurol.*, **20**, 758–763.
67. Claudepierre, T., Paques, M., Simonutti, M., Buard, I., Sahel, J., Maue, R.A., Picaud, S. and Pfrieger, F.W. (2010) Lack of Niemann-Pick type C1 induces age-related degeneration in the mouse retina. *Mol. Cell Neurosci.*, **43**, 164–176.
68. Hovakimyan, M., Meyer, A., Lukas, J., Luo, J.K., Gudziol, V., Hummel, T., Rolfs, A., Wree, A. and Witt, M. (2013) Olfactory deficits in Niemann–Pick type C1 (NPC1) disease. *Plos One*, **8**, e82216.
69. Pacheco, C.D., Kunkel, R. and Lieberman, A.P. (2007) Autophagy in Niemann-Pick C disease is dependent upon Beclin-1 and responsive to lipid trafficking defects. *Hum. Mol. Genet.*, **16**, 1495–1503.
70. Sarkar, S., Carroll, B., Buganim, Y., Maetzel, D., Ng, A.H.M., Cassady, J.P., Cohen, M.A., Chakraborty, S., Wang, H., Spooner, E. *et al.* (2013) Impaired autophagy in the lipid-storage disorder Niemann-Pick type C1 disease. *Cell Rep.*, **5**, 1302–1315.
71. Meske, V., Erz, J., Priesnitz, T. and Ohm, T.G. (2014) The autophagic defect in Niemann-Pick disease type C neurons differs from somatic cells and reduces neuronal viability. *Neurobiol. Dis.*, **64**, 88–97.
72. Pampliega, O., Orhon, I., Patel, B., Sridhar, S., Diaz-Carretaro, A., Beaui, I., Codongo, P., Satir, B.H., Satir, P. and Cuervo, A.M. (2013) Functional interaction between autophagy and ciliogenesis. *Nature*, **502**, 194–200.
73. Loftus, S.K., Morris, JA. Carstea, ED., Gu, J.Z., Cummings, C., Brown, A., Ellison, J., Ohno, K., Rosenfeld, M.A., Tagle, D.A., Pentchev, P.G. and Pavan, W.J. (1997) Murine model of Niemann-Pick C disease: mutation in a cholesterol homeostasis gene. *Science*, **11**, 232–235.
74. Palladino, G., Loizzo, S., Fortuna, A., Canterini, S., Palombi, F., Erickson, R.P., Mangia, F. and Fiorenza, M.T. (2015) Visual evoked potentials of Niemann-Pick type C1 mice reveal an impairment of the visual pathway that is rescued by 2-hydroxypropyl-ß-cyclodextrin. *Orphanet. J. Rare Dis.,* **12**, *100-133*,
75. Wang, W., Wu, T. and Kirschner, M.W. (2014) The master cell cycle regulator APC-Cdc20 regulates ciliary length and disassembly of the primary cilium. *e-Life*, **3**, e03083.
76. Livak, K.J. and Schmittgen, K.J. (2001) Analysis of relative gene expression data using real-time quantitative PCR and the 2(-Delta Delta C (T)) Method. *Methods*, **25**, 402–408.
77. Canterini, S., Carletti, V., Nusca, S., Mangia, F. and Fiorenza, M.T. (2013) Multiple TSC22D4 iso-/phospho-glycoforms display idiosyncratic subcellular localizations and interacting protein partners. *FEBS J.*, **280**, 1320–1329.

Downloaded from https://academic.oup.com/hmg/article/26/12/2277/3098490 by U.S. Department of Justice user on 17 August 2022